Int. J. Heat Mass Transfer. Vol. 34, No. 9, pp. 2207–2218, 1991
Printed in Great Britain

0017-9310/91 $3.00 + 0.00

The effect of asymmetric heating on the onset of thermal instability in the thermal entrance region of a parallel plate channel

F. S. LEE and G. J. HWANG†

Department of Power Mechanical Engineering, National Tsing Hua University, Hsinchu, Taiwan 30043, R.O.C.

(*Received* 6 *July* 1990 *and in final form* 18 *October* 1990)

Abstract—This paper presents a time-dependent linear analysis on the onset of thermal instability of fully developed laminar flow in the thermal entrance region of a horizontal parallel plate channel heated asymmetrically; where the lower plate, upper plate and inlet are subjected to three different constant temperatures. The heating of the upper plate causes a thermal stratification, but the heating of the lower plate introduces a thermal destabilization. With the three different inlet, upper plate and lower plate temperatures, six heating configurations for the horizontal parallel plate channel are analysed and only three representative unstable heating configurations are shown. A criterion $\partial/\partial t = 0$ with $\partial/\partial x \neq 0$ for the determination of the critical condition marking the onset of longitudinal vortex rolls yields results that agree well with the existing experimental data in comparison with the criterion $\partial/\partial x = 0$ used previously. The critical Rayleigh numbers and the corresponding critical wave numbers for the three unstable heating configurations with $Pr = 0.7$ and 7.0 are presented.

1. INTRODUCTION

IT IS WELL known that buoyancy effects strongly influence the hydrodynamic and thermal developments of horizontal laminar internal flows. The buoyancy driven secondary flow can enhance the forced convection heat transfer in compact heat exchangers, flat plate solar collectors and in the cooling of electronic components. Since the thermal instability will occur in the development region, the mixed convection effect is also important in a horizontal chemical vapour deposition (CVD) reactor. The buoyancy force on the laminar internal flow induces a secondary flow which can reduce the thermal entry length, enhance the heat transfer rate and promote an early transition to turbulence. The thermal instability of mixed convection in horizontal parallel plate channels or rectangular ducts has been studied theoretically and experimentally by many investigators.

Mori and Uchida [1] applied a linear stability analysis to determine the onset of an infinitesimal disturbance in the form of longitudinal vortex rolls for fully developed laminar flow between parallel plates, with the bottom and top surfaces heated and cooled, respectively. The critical Rayleigh numbers corresponding to the onset of rolls of the first and the second type were determined. Nakayama *et al.* [2] studied the conditions marking the onset of longitudinal vortices for fully developed laminar flow between horizontal parallel plates with a non-linear basic temperature profile.

Using a linear stability theory, Hwang and Cheng [3] determined the conditions marking the onset of longitudinal vortex rolls in the thermal entrance region of a horizontal parallel plate channel heated from below. They found that for $Pr \geqslant 0.7$ the flow is more stable in the thermal entrance region than that in the fully developed region, but the situation is just the opposite for small Prandtl numbers, say $Pr \leqslant 0.2$. Cheng and Wu [4] studied the effect of axial heat conduction on the onset of instability of a channel flow. They found that the transverse vortex disturbances were preferred over the longitudinal vortex disturbances for $Pe \leqslant 1$ and $Pr \geqslant 1$ (low Re) in the developing region upstream and downstream of the thermal entrance. Mahaney *et al.* [5] employed a vectorized finite difference marching technique and calculations were performed for water in the combined entry region. They found that as Gr^* increases, the onset of instability is advanced and heat transfer enhancement relative to the forced convection limit is increased. The number of vortices increases with the increasing Grashof number and aspect ratio.

Akiyama *et al.* [6] studied experimentally the onset of longitudinal vortex rolls for the fully developed laminar flow of air between two horizontal flat plates subjected to a uniform axial wall temperature gradient. Ostrach and Kamotani [7] measured the heat transfer rate for a fully developed forced convection flow between two horizontal plates. Hwang and Liu [8] studied the onset of longitudinal vortices due to the buoyant force in the thermal entrance region of a horizontal parallel plate channel heated from below to verify the theoretical prediction [3]. They observed that the critical Rayleigh number from flow visu-

† Author to whom all correspondence should be addressed.

NOMENCLATURE

a wave number of longitudinal vortices, $2\pi h/\lambda$
D dimensionless continuity equation
g gravitational acceleration
Gr Grashof number, $\beta g \Delta T h^3/\nu^2$
h distance between two parallel plates
n number of time step
NI, NJ number of grids in streamwise and normal directions
p', P, P_b perturbation, resultant and basic pressures
Pe Peclet number, $U_m h/\kappa$
Pr Prandtl number, ν/κ
Ra Rayleigh number, $\beta g \Delta T h^3/\nu\kappa$
Re Reynolds number, $U_m h/\nu$
t dimensionless time
t', T, T_b perturbation, resultant and basic temperatures
T_{max}, T_{min} maximum, minimum of basic temperatures of inlet, lower plate and upper plate
ΔT characteristic temperature difference, $T_{max} - T_{min}$
u, v, w dimensionless amplitude functions of perturbation velocity in the x-, y- and z-directions
u', v', w' streamwise, normal and spanwise perturbation velocities
$\hat{u}$, $\hat{v}$, $\hat{w}$ dimensionless streamwise, normal and spanwise perturbation velocities
U, V, W resultant streamwise, normal and spanwise velocities
U_b, U_m streamwise basic and mean velocities
x, y, z dimensionless streamwise, normal and spanwise coordinates, $X(Pe\,h)$, Y/h and Z/h
X, Y, Z streamwise, normal and spanwise coordinates.

Greek symbols
β volumetric coefficient of thermal expansion
θ dimensionless perturbation temperature
κ thermal diffusivity of fluid
λ wavelength
ν kinematic viscosity of fluid
ρ density of fluid
τ time
ϕ_u dimensionless basic streamwise velocity
ϕ_θ dimensionless basic temperature
ϕ_θ^I, ϕ_θ^L, ϕ_θ^U dimensionless basic temperatures at inlet, lower plate and upper plate.

Subscripts
b basic flow quantity
c characteristic quantity
m mean flow.

Superscripts
′ perturbation quantity
^ dimensionless perturbation quantity
* critical condition
0 initial state
— r.m.s. value
I inlet
L lower plate
U upper plate.

alization was 1.4–10 times higher than the theoretical results [3]. Kamotani and co-workers [9, 10] performed experiments for air flow in the thermal entrance region of a horizontal parallel plate channel. They determined the onset of thermal instability from visualization of the secondary flow. Measurements of Nusselt numbers and temperature distributions indicated that the critical Rayleigh numbers agree reasonably with previous experiments [8]. Incropera *et al.* [11] detected the secondary flow by flow visualization and heat transfer measurement for water flow. They found that the wavelength of the vortex decreases continuously with increasing Gr_D^*. Maughan and Incropera [12] studied the effect of surface heat flux and channel orientation on the local Nusselt number. The onset of instability was delayed by decreasing the Grashof number and/or by increasing the Reynolds number and inclination angle. Chiu and Rosenberger [13] measured the onset point positions of instability from the velocity profile by laser Doppler anemometry.

Most of the previous studies examined the thermal instability in parallel plate channels and rectangular ducts with the thermal condition of heating from below. There were some papers that dealt with the effect of asymmetric heating on heat transfer. Osborne and Incropera [14] performed an experiment to determine the hydrodynamic and thermal condition in laminar water flow between horizontal parallel plates with a uniform asymmetric heat flux. Flow visualization and temperature measurements revealed the existence of a buoyancy driven flow which strongly influenced bottom plate conditions, but had a weak influence on top plate conditions. Heat transfer at the

top plate was dominated by forced convection, while heat transfer at the bottom plate was characterized by mixed convection. Incropera and Schutt [15] performed a numerical investigation to determine the nature and effect of thermally driven secondary flow in a horizontal channel with heated top and bottom surfaces and insulated side walls, with top-to-bottom surface heat flux ratio ($-1.0 \leqslant q_t/q_b \leqslant 5.0$). Kurosaki and Satoh [16] presented a numerical study concerning the effects of non-uniform heating on the heat transfer of a thermally undeveloped gas flow in a horizontal rectangular duct; a vertical side wall is uniformly heated and the other walls are insulated. Mahaney *et al.* [17] evaluated the effects of buoyancy on forced flow in a horizontal duct of aspect ratio $A = 2$ numerically. They considered eight distinct heating conditions for which selective duct surfaces are either adiabatic or uniformly heated, with identical conditions applied to the side wall. It is obvious that the effect of asymmetric heating on the thermal instability has received relatively less attention in spite of its importance in practical application such as flat plate solar collectors or heat exchangers. Furthermore, one notes that the study on the effects of heating condition on the onset of instability in the thermal entrance region has not been found in the literature.

The objective of this paper is to predict the effect of asymmetric heating conditions on the onset of thermal instability in the thermal entrance region of a parallel plate channel. The lower plate, upper plate and inlet are subjected to three different constant temperatures. The heating of the upper plate causes a thermal stratification, but the heating of the lower plate introduces a thermal destabilization. With the three different inlet, upper plate and lower plate temperatures, six heating configurations for the horizontal parallel plate channel are analysed and only three representative unstable heating configurations are found. In this paper a transient three-dimensional linear stability theory is used to determine the onset of thermal instability. The perturbation modes are expressed as time-dependent and functions of space variables X, Y and Z. Therefore, normalized transient perturbation equations in the normal and streamwise direction are derived, and then solved to determine the neutral stability condition by the criterion $\partial/\partial t = 0$ with non-zero streamwise derivatives.

2. THEORETICAL ANALYSIS

Consider a fully developed laminar flow of an incompressible viscous fluid in the thermal entrance region between horizontal parallel plates with gap h, where the lower plate and the upper plate are maintained at uniform temperatures T_L and T_U, respectively, for $X \geqslant 0$. The inlet fluid temperature is kept at a constant temperature T_I. The thermodynamic properties of fluid are assumed constant and the Boussinesq approximation is used. The physical configuration and coordinate system are shown in Fig. 1.

The governing equations for the basic flow are

$$U_b \frac{\partial T_b}{\partial X} = \kappa \left(\frac{\partial^2 T_b}{\partial X^2} + \frac{\partial^2 T_b}{\partial Y^2} \right) \tag{1}$$

$$U_b = 6U_m \left[\left(\frac{Y}{h} \right) - \left(\frac{Y}{h} \right)^2 \right] = U_m \phi_u \tag{2}$$

where U_m is the mean velocity and ϕ_u a dimensionless basic velocity function. By introducing dimensionless variables $x = X/(Pe\, h)$, $y = Y/h$, $\phi_\theta = (T_b - T_{min})/\Delta T$ and the parameter $Pe = U_m h/\kappa$, the following normalized equation results:

$$\phi_u \frac{\partial \phi_\theta}{\partial x} = \frac{1}{Pe^2} \frac{\partial^2 \phi_\theta}{\partial x^2} + \frac{\partial^2 \phi_\theta}{\partial y^2}. \tag{3}$$

The boundary conditions are

$$\begin{aligned} &\phi_\theta(x, 0) = \phi_\theta^L \\ &\phi_\theta(x, 1) = \phi_\theta^U \end{aligned} \quad \text{for } x \geqslant 0$$

$$\begin{aligned} &\phi_\theta(0, y) = \phi_\theta^I \\ &\phi_\theta(\infty, y) = \phi_\theta^L + y(\phi_\theta^U - \phi_\theta^L) \end{aligned} \quad \text{for } 0 \leqslant y \leqslant 1. \tag{4}$$

3. PERTURBATION EQUATIONS

For forced convection flow in the thermal entrance region, a non-linear basic temperature distribution exists in the normal direction near the lower and upper plates. The distribution becomes linear in the thermally fully developed region. The perturbation quantities are superimposed on the basic flow quantities as follows:

$$\begin{aligned} U &= U_b(Y) + u'(X, Y, Z, \tau) \\ V &= v'(X, Y, Z, \tau) \\ W &= w'(X, Y, Z, \tau) \\ P &= P_b(X, Y) + p'(X, Y, Z, \tau) \\ T &= T_b(X, Y) + t'(X, Y, Z, \tau). \end{aligned} \tag{5}$$

The above perturbation quantities are considered as functions of the space variables X, Y and Z and time variable τ. By substituting the resultant velocities, pressure and temperature (5) into the conservation equations for mass, momentum and energy, and subtracting the basic flow equations, we have the following linearized perturbation equations:

$$\frac{\partial u'}{\partial X} + \frac{\partial v'}{\partial Y} + \frac{\partial w'}{\partial Z} = 0 \tag{6}$$

$$\frac{\partial u'}{\partial \tau} + U_b \frac{\partial u'}{\partial X} + v' \frac{\partial U_b}{\partial Y} = -\frac{1}{\rho} \frac{\partial p'}{\partial X} + \nu \nabla_1^2 u' \tag{7}$$

$$\frac{\partial v'}{\partial \tau} + U_b \frac{\partial v'}{\partial X} = -\frac{1}{\rho} \frac{\partial p'}{\partial Y} + \nu \nabla_1^2 v' + \beta g t' \tag{8}$$

$$\frac{\partial w'}{\partial \tau} + U_b \frac{\partial w'}{\partial X} = -\frac{1}{\rho} \frac{\partial p'}{\partial Z} + \nu \nabla_1^2 w' \tag{9}$$

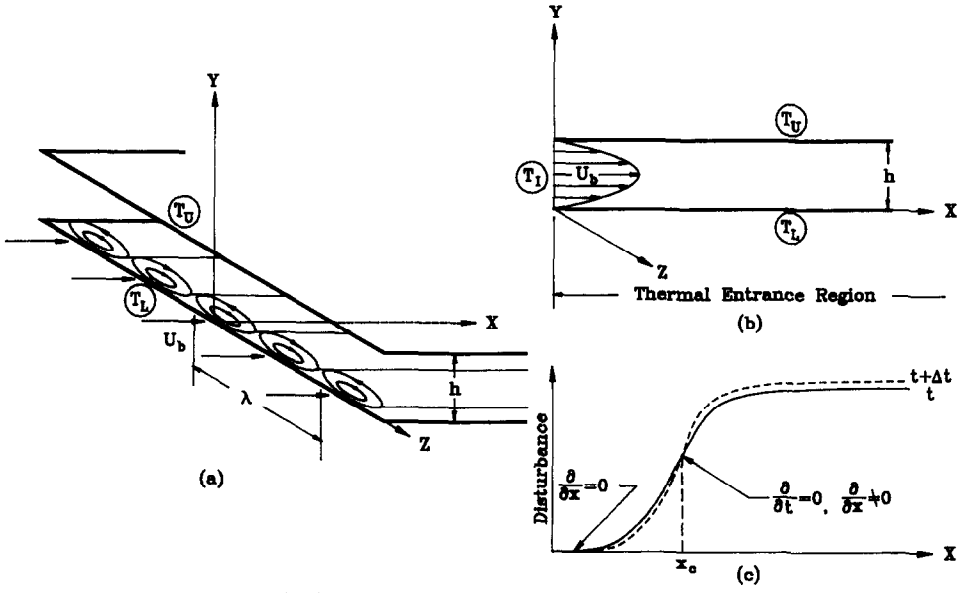

FIG. 1. Physical configuration and coordinate system.

$$\frac{\partial t'}{\partial \tau}+U_b\frac{\partial t'}{\partial X}+u'\frac{\partial T_b}{\partial X}+v'\frac{\partial T_b}{\partial Y}=\kappa\nabla_1^2 t' \qquad (10)$$

where

$$\nabla_1^2=\frac{\partial^2}{\partial X^2}+\frac{\partial^2}{\partial Y^2}+\frac{\partial^2}{\partial Z^2}.$$

After introducing the following dimensionless variables and parameters:

$$X=[Pe\cdot h]x,\quad Y=[h]y,\quad Z=[h]z,$$
$$u'=[U_m]\hat{u},\quad v'=[U_m]\hat{v},\quad w'=[U_m]\hat{w},$$
$$U_b=[U_m]\phi_u,\quad T_b-T_{min}=[\Delta T]\phi_\theta,\quad t'=[\Delta T]\hat{\theta},$$
$$\tau=[t_c]t,\quad p'=[p_c]\hat{p}$$

where

$$\Delta T=T_{max}-T_{min},\quad t_c=h^2/\nu$$
$$p_c=\rho\nu U_m/h \quad\text{and}\quad Ra=\beta g\Delta T h^3/\kappa\nu$$

the dimensionless perturbation equations become

$$\frac{1}{Pe}\frac{\partial\hat{u}}{\partial x}+\frac{\partial\hat{v}}{\partial y}+\frac{\partial\hat{w}}{\partial z}=0 \qquad (11)$$

$$\frac{\partial\hat{u}}{\partial t}+\frac{1}{Pr}\phi_u\frac{\partial\hat{u}}{\partial x}+\frac{Pe}{Pr}\hat{v}\frac{\partial\phi_u}{\partial y}=-\frac{1}{Pe}\frac{\partial\hat{p}}{\partial x}+\nabla_2^2\hat{u} \qquad (12)$$

$$\frac{\partial\hat{v}}{\partial t}+\frac{1}{Pr}\phi_u\frac{\partial\hat{v}}{\partial x}=-\frac{\partial\hat{p}}{\partial y}+\nabla_2^2\hat{v}+\frac{Ra}{Pe}\hat{\theta} \qquad (13)$$

$$\frac{\partial\hat{w}}{\partial t}+\frac{1}{Pr}\phi_u\frac{\partial\hat{w}}{\partial x}=-\frac{\partial\hat{p}}{\partial z}+\nabla_2^2\hat{w} \qquad (14)$$

$$Pr\frac{\partial\hat{\theta}}{\partial t}+\phi_u\frac{\partial\hat{\theta}}{\partial x}+\hat{u}\frac{\partial\phi_\theta}{\partial x}+Pe\,\hat{v}\frac{\partial\phi_\theta}{\partial y}=\nabla_2^2\hat{\theta} \qquad (15)$$

where

$$\nabla_2^2=\frac{1}{Pe^2}\frac{\partial^2}{\partial x^2}+\frac{\partial^2}{\partial y^2}+\frac{\partial^2}{\partial z^2}.$$

The perturbation modes are expressed as time-dependent and functions of space variables. The following disturbance forms for longitudinal vortex rolls are chosen:

$$\hat{u}(x,y,z,t)=u(x,y,t)\cdot\exp(iaz)$$
$$\hat{v}(x,y,z,t)=v(x,y,t)\cdot\exp(iaz)$$
$$\hat{w}(x,y,z,t)=w(x,y,t)\cdot i\cdot\exp(iaz)$$
$$\hat{p}(x,y,z,t)=p(x,y,t)\cdot\exp(iaz)$$
$$\hat{\theta}(x,y,z,t)=\theta(x,y,t)\cdot\exp(iaz) \qquad (16)$$

where $a=2\pi h/\lambda$ is the wave number of the longitudinal vortices. The manipulation of a different form of $\hat{w}$ from those of $\hat{u}$, $\hat{v}$, $\hat{p}$ and $\hat{\theta}$ is based on the consideration of the continuity equation. It should be noted that these roll-type disturbances are taken to be periodic in the z-direction, with u, v, w, p and θ as the amplitude functions depending on x, y and t. It is noted that in refs. [3, 4, 18, 19] a steady two-dimensional disturbance $\hat{f}(y,z)=f(y)\cdot\exp(iaz)$ is assumed and the neutrally stable condition at the onset point is indicated by $\partial\hat{f}/\partial x=0$. A steady three-dimensional perturbation $\hat{f}(x,y,z)=f(y)\cdot\exp(iaz)$ with the assumption of a large Prandtl number is used by Yoo *et al.* [20] for a mixed convection on an isothermal horizontal plate. In the present study, the perturbation functions are presumed as functions of x, y, z and t. The onset position of vortex instability is characterized by $\partial\hat{f}/\partial t=0$ with $\partial\hat{f}/\partial x\neq 0$ [21] which is different from $\partial\hat{f}/\partial x=0$ for the two-dimensional disturbances.

After substituting the disturbance form (16) into equations (11)–(15), one obtains the following equations in the x–y plane for the time-dependent amplitude functions:

$$\frac{1}{Pe}\frac{\partial u}{\partial x}+\frac{\partial v}{\partial y}-aw=0 \tag{17}$$

$$\frac{\partial u}{\partial t}+\frac{1}{Pr}\phi_u\frac{\partial u}{\partial x}+\frac{Pe}{Pr}v\frac{\partial \phi_u}{\partial y}=-\frac{1}{Pe}\frac{\partial p}{\partial x}+\nabla^2 u \tag{18}$$

$$\frac{\partial v}{\partial t}+\frac{1}{Pr}\phi_u\frac{\partial v}{\partial x}=-\frac{\partial p}{\partial y}+\nabla^2 v+\frac{Ra}{Pe}\theta \tag{19}$$

$$\frac{\partial w}{\partial t}+\frac{1}{Pr}\phi_u\frac{\partial w}{\partial x}=-ap+\nabla^2 w \tag{20}$$

$$Pr\frac{\partial \theta}{\partial t}+\phi_u\frac{\partial \theta}{\partial x}+u\frac{\partial \phi_\theta}{\partial x}+Pe\,v\frac{\partial \phi_\theta}{\partial y}=\nabla^2\theta \tag{21}$$

where

$$\nabla^2=\frac{1}{Pe^2}\frac{\partial^2}{\partial x^2}+\frac{\partial^2}{\partial y^2}-a^2.$$

The equation for the pressure amplitude function is obtained after some manipulations and incorporating the dimensionless equations (17)–(20)

$$\nabla^2 p=-\frac{\partial D}{\partial t}+\nabla^2 D-\frac{1}{Pr}\phi_u\frac{\partial D}{\partial x}-\frac{2}{Pr}\frac{\partial v}{\partial x}\frac{\partial \phi_u}{\partial y}+\frac{Ra}{Pe}\frac{\partial \theta}{\partial y} \tag{22}$$

where

$$D=\frac{1}{Pe}\frac{\partial u}{\partial x}+\frac{\partial v}{\partial y}-aw.$$

It is noted that the present study utilizes the reduced two-dimensional equations (18)–(22) instead of the three-dimensional ones (11)–(15), and solves the unabridged pressure equation (22) in comparison with the simplified equations used for the determination of p in the SIMPLE and SIMPLER methods [22]. In the present study, the assumption of a large Peclet number is also used. It is easy to prove that a set of governing perturbation equations without the parameter Pe can be obtained from equations (17) to (22) by transforming $\theta = Pe\cdot\tilde{\theta}$, $u = Pe\cdot\tilde{u}$ and keeping the same v, w, t, p, and assuming $1/Pe^2 \to 0$ for a large Peclet number. Furthermore, a numerical experiment was also carried out for the solution of a large Peclet number; for instance, $Pe = 175$ and 350 were selected for computation and no appreciable difference was found.

The appropriate boundary conditions of the perturbations quantities are

$$u=v=w=\theta=0 \qquad \text{at } y=0 \text{ and } 1$$

$$u=v=w=\theta=0 \qquad \text{at } x=0$$

$$\frac{\partial u}{\partial x}=\frac{\partial v}{\partial x}=\frac{\partial w}{\partial x}=\frac{\partial \theta}{\partial x}=\frac{\partial p}{\partial x}=0 \qquad \text{at } x=1 \tag{23}$$

and the initial conditions of the perturbation quantities are

$$u=v=w=\theta-\theta^0=p=0 \qquad \text{at } t=0 \tag{24}$$

where θ^0 is set as 1×10^{-10} in the present computation. It is noted that the pressure at the walls and the inlet are not listed above. Following the procedure in ref. [23] the boundary conditions for the pressure equation (22) can be derived directly from the momentum equations (18) and (19), which must be consistent with the vanishing of the perturbation velocities u and v at the walls and inlet.

It may be interesting to see the effect of Pe on the onset of thermal instability. Therefore, the streamwise convection and diffusion terms of the governing equations are not neglected in this study. The convection terms with the coefficient $1/Pr$ also show that the Prandtl number plays an important role on the onset of thermal instability.

4. SOLUTION PROCEDURE

The numerical solution of the governing equations is based on the Mark and Cell (MAC) scheme [23] with a staggered grid system. The velocity amplitude functions u, v are calculated at the points on the surface of a control volume, while the velocity, pressure and temperature amplitude functions are solved at the grid point in the control volume. Since the streamwise convection terms in the governing equations are first-order derivatives with a factor of $1/Pr$, equations (18)–(20) will become stiff when the Prandtl number is small, the power law scheme [22] is employed for the inertia–viscous and conduction–convection terms. Equation (22) is a Poisson equation which can be solved by a successive over-relaxation iteration method. The explicit forward time marching is utilized to treat the time-dependent form.

It is seen in equation (19) that the buoyancy term is a driving force which supplies the energy to increase the perturbation velocity, and then the perturbation temperature in equation (21) is promoted by the normal convection but suppressed by the streamwise convection. In computation one can modify the Rayleigh number at each time step by a linear extrapolation according to the perturbation temperature amplitudes at the two previous time steps on a specified streamwise position. This process is repeated until a minimum value of the Rayleigh number is obtained.

The basic concept of this approach is that the unstable region is located downstream of the onset position of instability, and the perturbation quantities in the unsteady linear perturbation equations can grow endlessly as time increases. The stable region is located upstream, and the initial perturbations decrease continuously. Based on this concept an initial uniform disturbed temperature θ^0 and an initial guessed Rayleigh number Ra^0 are given for a wave number a. During the time marching process, the Rayleigh number is modified at each time step, until

the perturbation temperature amplitude and the values of the minimum Rayleigh number meet the following convergence criteria for a dimensionless specified streamwise position:

$$\left|\frac{\bar{T}_{x,t}-\bar{T}_{x,t-\Delta t}}{\bar{T}_{x,t}}\right| \leqslant \varepsilon \qquad (25)$$

for perturbation temperature amplitude, where $\bar{T}_{x,t}$ is the r.m.s. value of the temperature amplitude at time t on a specified dimensionless streamwise position x, and $\varepsilon = 1\times10^{-3}$–$5\times10^{-5}$ in the study, and

$$Ra_{t-\Delta t}+Ra_{t+\Delta t}-2Ra_t > 0 \quad \text{and}$$
$$Ra_{t-\Delta t} > Ra_t < Ra_{t+\Delta t} \qquad (26)$$

for the determination of the minimum Rayleigh number. By changing the wave number, one can determine the smallest value among these minimum Rayleigh numbers. The smallest value of these minimum Rayleigh numbers is the critical Rayleigh number Ra^* and the corresponding wave number is the critical wave number a^*. The specified streamwise position is the onset position of the thermal instability.

The main objective of this study is to determine the critical condition of the onset of thermal instability for a specified streamwise position. The grid is uniform in the normal direction and nonuniform in the streamwise direction to save computation time. A fine mesh near the inlet region is employed to obtain better accuracy in the solution. Table 1 shows a typical result of numerical experiments for $Pe = 175$. Dimensionless time increments of 0.12×10^{-3} and 0.16×10^{-3}, initial Rayleigh numbers of 8.0×10^4, 1.6×10^5 and 3.0×10^5, initial perturbation temperatures of 1.0×10^{-9}, 1.0×10^{-10} and 1.0×10^{-11} and grid sizes of 80×23, 80×28 and 101×23 are used to perform the numerical calculations. One finds that the difference in numerical results decreases as the onset streamwise position moves downstream. For example the results appear at $x = 0.01$ with a maximum difference of 2.0%, but the difference at $x \geqslant 0.10$ is less than 1%. Note that the magnitude of the initial guessed perturbation temperature will not affect the determination of critical conditions, since linear perturbation equations are employed in the present analysis.

Table 1. Numerical experiments for $Pe = 175$

	Ra^*		
	Onset position (x^*)		
	0.01	0.05	0.10
Typical calculation†	62718	8285	3545
$\Delta t = 0.12\times10^{-3}$	63522	8362	3563
$Ra^0 = 8.0\times10^4$	62656	8171	3535
$Ra^0 = 3.0\times10^5$	61333	8369	3548
$\theta^0 = 1.0\times10^{-11}$	62718	8285	3545
$\theta^0 = 1.0\times10^{-9}$	62718	8285	3545
$NI\times NJ = 101\times23$	63317	8174	3516
$NI\times NJ = 80\times28$	63837	8372	3570

† $\Delta t = 0.16\times10^{-3}$, $Ra^0 = 1.6\times10^5$, $\theta^0 = 1.0\times10^{-10}$, $NI\times NJ = 80\times23$.

5. RESULTS AND DISCUSSION

To begin with, the feasibility of the numerical method proposed in this paper is confirmed by applying it to the conventional thermal instability in the thermal entrance region of a horizontal parallel plate channel, where the lower plate is heated isothermally, i.e. $\phi_\theta^U = \phi_\theta^I = 0$ and $\phi_\theta^L = 1.0$. The instability curves were obtained and compared with the previous studies. Figure 2 shows the critical Rayleigh number Ra^* marking the onset of instability along the streamwise direction. The previous theoretical and experimental data are also plotted for comparison. The theoretical prediction of ref. [3] is the first investigation of such a problem, and the critical condition $\partial/\partial x = 0$ was used in this approach. Because infinitesimal disturbances are difficult to detect experimentally, the critical condition can be determined only after the amplitudes of perturbation quantities have grown large enough to be detected. It is thus understandable that the difference between the previous theoretical prediction [3] and the experimental data [8–10, 12, 13] are more than one order of magnitude nearer the inlet region. On the other hand, the present numerical results utilizing an instability criterion $\partial/\partial t = 0$ with $\partial/\partial x \neq 0$ show a good agreement with the existing experimental results [8–10, 12, 13]. The physical basis for this difference can be explained by using Fig. 1(c). X-Dependent disturbances which satisfy the boundary conditions shown in equation (23) are employed in the present study. The critical Rayleigh number Ra^* at x_c is determined by the criteria $\partial/\partial t = 0$ and $\partial/\partial x \neq 0$. In the previous studies [3, 14, 18, 19] the critical condition is determined at the upstream of x_c by using the criterion $\partial/\partial x = 0$ which uses x-independent disturbances. The numerical procedure described here is therefore capable of handling the prediction of the effect of asymmetric heating on thermal instability.

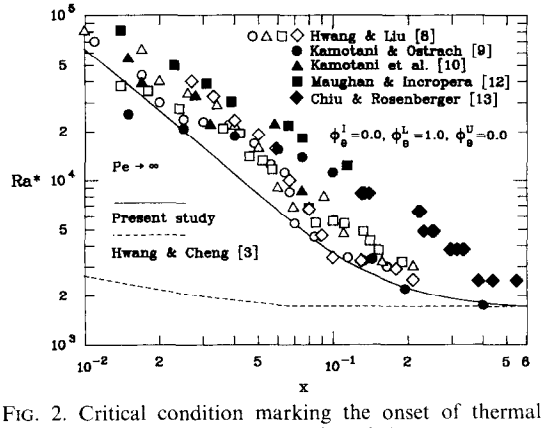

FIG. 2. Critical condition marking the onset of thermal instability for heating from below.

Figure 3 presents six different heating configurations for the horizontal parallel plate channel. In each configuration, there are three constant boundary temperatures, i.e. the lower plate temperature T_L, the upper plate temperature T_U and the inlet temperature T_I. Three different temperatures T_{max}, T_{mid} and T_{min} ($T_{max} > T_{mid} > T_{min}$) assigned to the highest, intermediate and the lowest temperature of T_L, T_U and T_I for different arrangements yield the six different heating configurations. In Fig. 3 for heating configuration (A) there is no adverse temperature gradient in the flow field. The system is theoretically stable and no secondary vortex flow occurs. For configuration (B), an adverse temperature gradient exists in the gravitational direction and the system presents a theoretically unstable condition. If the Rayleigh number is high enough, a secondary flow occurs somewhere in the region and grows downstream. For configurations (C) and (D) the adverse temperature gradients exist only near the lower plate and the upper plate, respectively. For these configurations, the system is potentially unstable near the lower or upper plate. For configurations (E) and (F), the systems are stable except for the small regions close to the inlet where the adverse temperature gradients exist. For configuration (E) with a sufficiently high Rayleigh number, a secondary flow may occur near the lower plate but will not extend too far from the inlet, and will decay and eventually disappear downstream. A similar phenomenon appears for configuration (F) except that the secondary flow will occur near the upper plate. Hereinafter the dimensional basic flow temperature T_b is changed to a dimensionless form ϕ_θ by the transformation of $\phi_\theta = (T_b - T_{min})/\Delta T$. Temperatures of the upper plate, lower plate and inlet region are denoted by ϕ_θ^U, ϕ_θ^L and ϕ_θ^I, respectively.

The profiles of the perturbation amplitude quantities u, v, w and θ on the x–y plane for a typical case of configuration (B) are shown in Fig. 4. These data are obtained at the final time step for $Pr = 0.7$, $Pe \to \infty$ and the onset position at $x = 0.05$. These shapes of the v and w profiles may be explained via the circulation pattern shown in Fig. 1 while the u profile may be explained in light of the v profile which drives low momentum fluid away from the lower plate and high momentum fluid toward the upper plate. It should be noted that these results correspond to the perturbation amplitude quantities only, while the actual value of the perturbation quantities as a function of z will be derived from equation (16). Since the basic flow with adverse temperature gradient in the gravitational direction induces an upward motion as a result of the buoyancy force, the perturbation quantity v is always positive. It is seen that these perturbation amplitude quantities are very small near the inlet, gradually increase along the streamwise direction, and become fully developed after a certain streamwise distance.

The profiles of perturbation amplitudes for configuration (C) on the same onset position and Pr are shown in Fig. 5. These perturbation amplitude quantities increase from the inlet region along the streamwise direction. After reaching maximum amplitudes, the perturbation quantities decrease gradually along the downstream direction, and then all of them

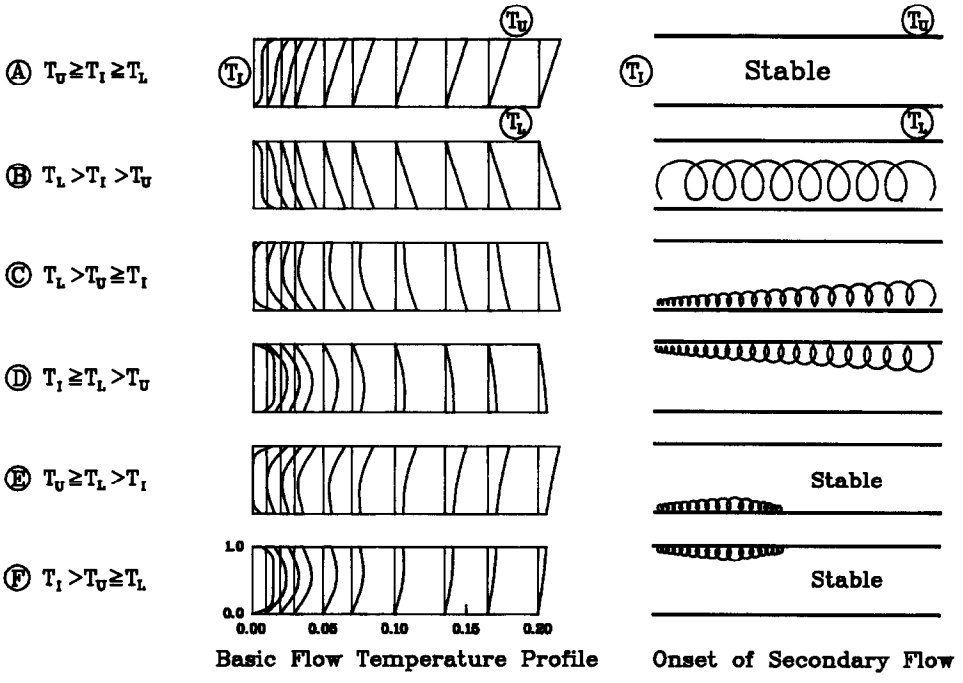

FIG. 3. Basic temperature profiles and various heating configurations.

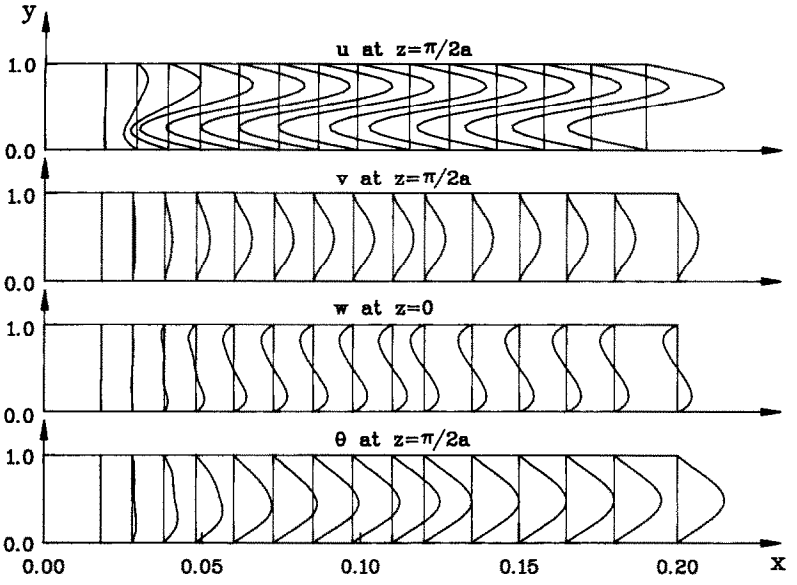

$\phi_\theta^I=0.4,\ \phi_\theta^L=1.0,\ \phi_\theta^U=0.0$

(x=0.05, Pr=0.7, Pe→∞)

FIG. 4. Perturbation amplitude profiles for configuration (B).

reach the fully developed values. Since the upper plate is also heated, the adverse temperature gradient near the lower plate is not so strong as to increase these amplitudes continuously for this configuration.

In Fig. 6, a case for configuration (E) is presented. The perturbation amplitude quantities initially increase along the streamwise direction. After reaching maximum values, these perturbation quantities decrease rapidly and eventually disappear downstream. This is because no adverse temperature gradient is present downstream of the onset position of instability. Lacking the support of buoyancy force, the secondary flow is suppressed. The vortex rolls exist only in part of the entrance region.

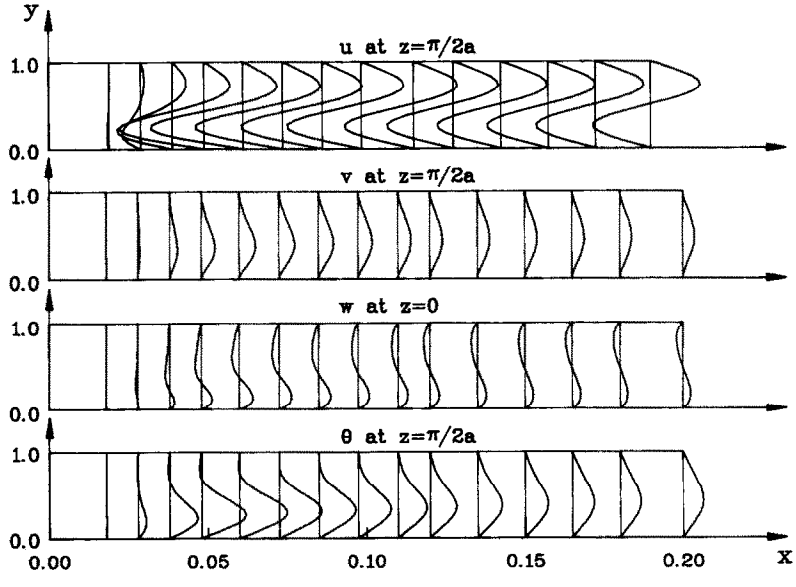

$\phi_\theta^I=0.0,\ \phi_\theta^L=1.0,\ \phi_\theta^U=0.4$

(x=0.05, Pr=0.7, Pe→∞)

FIG. 5. Perturbation amplitude profiles for configuration (C).

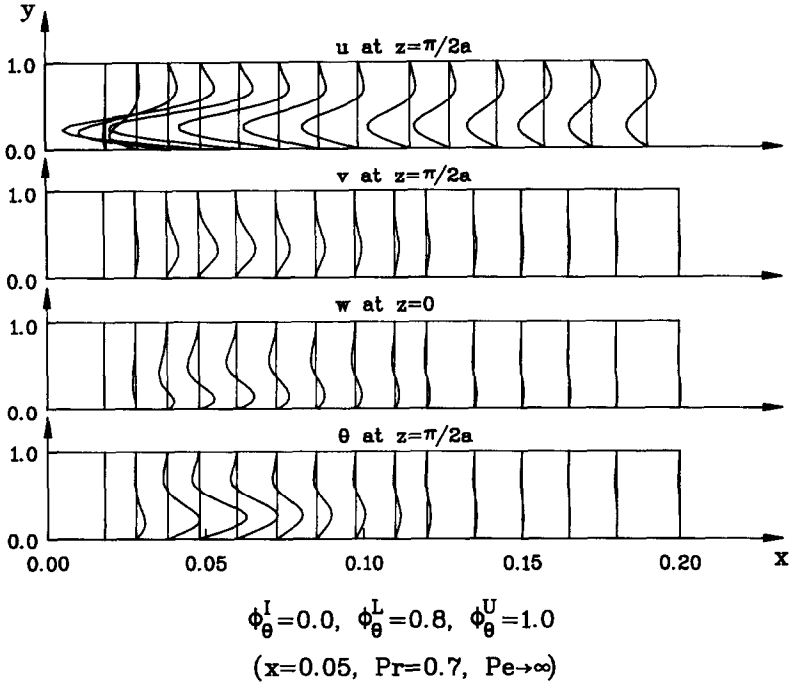

FIG. 6. Perturbation amplitude profiles for configuration (E).

Figure 7(a) shows the critical Rayleigh number Ra^* vs the dimensionless streamwise coordinate for the case corresponding to configuration (B) in Fig. 3. In this figure, the case $\phi_\theta^L > \phi_\theta^I > \phi_\theta^U$ is considered for $Pr = 0.7$ and 7.0. It is shown that as ϕ_θ^I increases from 0.0 to 0.5, the critical Rayleigh number for a fixed x increases gradually. For the case of $\phi_\theta^I = 0.5$, the equally-valued adverse temperature gradients near the lower and upper plates give the highest Ra^* in comparison with that for the other unequally-valued temperature gradients. It is indicated that the increasing inlet temperature from 0.0 to 0.5 has a stabilizing effect on the flow. This effect is more pronounced upstream than that downstream. Since they have the same adverse temperature gradients, the critical conditions are identical for the cases $\phi_\theta^I = 0.0$ and 1.0. The same reason applies to the cases of $\phi_\theta^I = 0.2$, 0.8 and 0.4, 0.6. It is seen in equations (18)–(20) that for fixed Pe and x, the streamwise direction inertia force, which suppresses the thermal instability, increases with the decrease in the Prandtl number, therefore, the increased stability of low Prandtl number flow is shown in Fig. 7(a).

Figure 7(b) shows the corresponding critical wave number a^* vs the dimensionless streamwise coordinate. The critical wave numbers decrease monotonically in the streamwise direction and all converge to the same limiting value. For a given Pr the case with a higher Ra^* has a smaller wave number than that of the lower Ra^*. This means that there are more vortex rolls for a more unstable flow. For a fixed x and Pr, the curve for $\phi_\theta^I = 0.5$ shows the smallest a^* or largest wavelength λ among the curves for

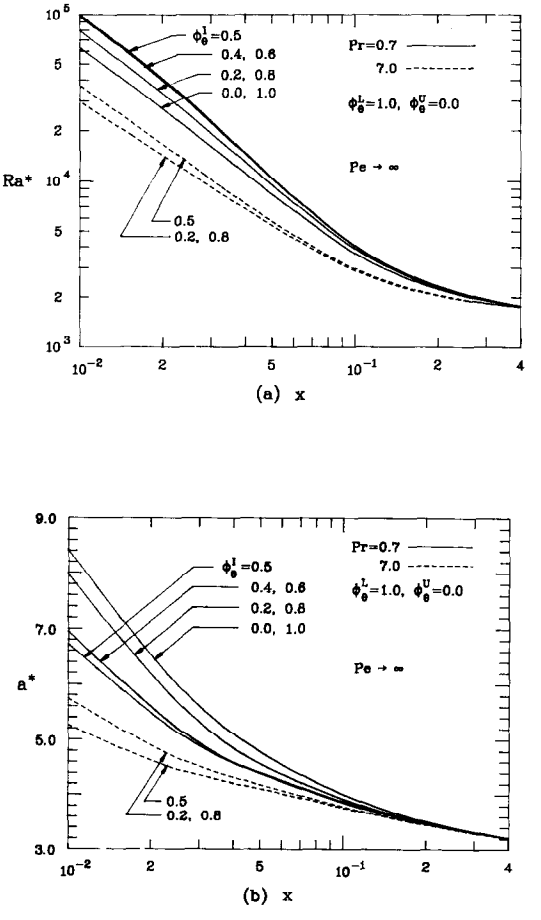

FIG. 7. (a) Ra^* vs x for configuration (B). (b) a^* vs x for configuration (B).

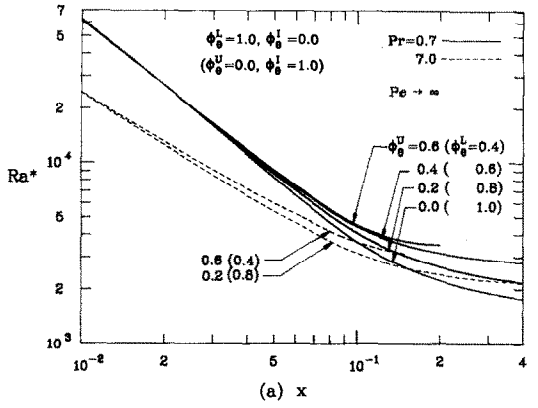

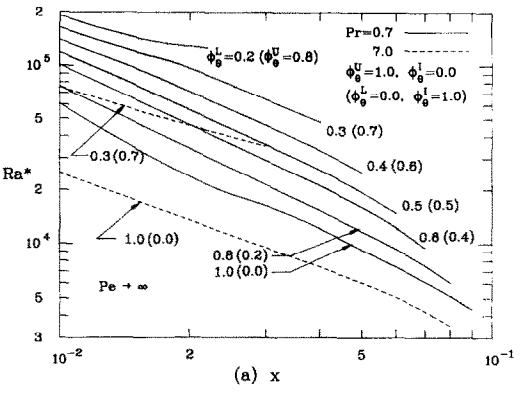

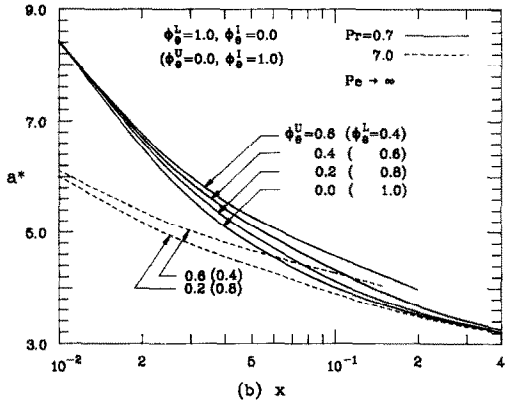

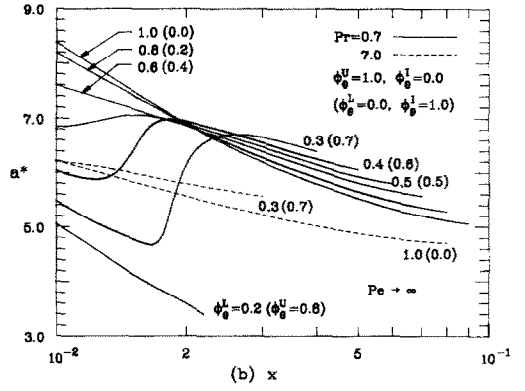

FIG. 8. (a) Ra^* vs x for configurations (C) and (D). (b) a^* vs x for configurations (C) and (D).

FIG. 9. (a) Ra^* vs x for configurations (E) and (F). (b) a^* vs x for configurations (E) and (F).

$\phi_\theta^I = 0.0$–1.0. The equally-valued temperature gradients near the lower and upper plates for the case of $\phi_\theta^I = 0.5$ allow the occupancy of the vortex rolls in the whole channel height. Because the cross-section of the vortex is nearly square, this gives the largest wavelength or the smallest wave number. For an increasing Pr, the wave number is decreased due to an increasing vortex size caused by the viscous force.

Figure 8(a) presents the critical conditions for configurations (C) and (D). The heating condition of configuration (D) is indicated in parentheses. Because they have the same adverse temperature gradient, the critical conditions are identical except that the secondary flow occurs near the lower plate or the upper plate. The heating of the upper plate in configuration (C) indicated by the values of $\phi_\theta^U = 0.0$–0.6 shows no effect on Ra^* in the region near the inlet, but presents a larger effect in the downstream direction. The critical Rayleigh number increases with an increase in ϕ_θ^U. It is also seen that the critical Rayleigh number is decreased with an increase in Pr due to a relatively large viscous force. For $\phi_\theta^U = 0.6$ the region downstream of the streamwise dimensionless positions $x = 0.20$ for $Pr = 0.7$ and $x = 0.15$ for $Pr = 7.0$, there is not enough buoyancy force to support the onset of secondary flow due to strong thermal stratification. Figure 8(b) presents the corresponding critical wave numbers a^* vs the dimensionless streamwise coordinate. It also shows that the critical wave number decreases monotonically along the streamwise direction. An increase in the upper plate heating will suppress the growth of vortex rolls near the upper plate. The corresponding wavelength decreases and the wave number increases as ϕ_θ^U increases.

Because the same adverse temperature gradient exists near the lower and upper plates, configurations (E) and (F) show the same critical conditions, Fig. 9(a) depicts these results. The heating condition of configuration (F) is presented in parentheses. In configuration (E) the upper plate thermal stratification is stronger than the lower plate thermal destabilization. There is no occurrence of secondary flow due to a thermally stable situation in some of the flow field. An increase in the lower plate heating will decrease the critical Rayleigh number. It is seen that a larger Pr also shows a smaller Ra^* in this configuration.

The corresponding critical wave number a^* vs the dimensionless streamwise coordinate for configurations (E) and (F) are presented in Fig. 9(b). It shows a quite different behaviour as compared with that shown in Figs. 7(b) and 8(b). Curves for $\phi_\theta^L = 0.6$, 0.8 and 1.0 decrease monotonically with an increase in x. For the other curves, a different trend is observed. The curves for $\phi_\theta^L = 0.3$ and 1.0 are selected as typical examples to explain the different behaviours of the critical wave numbers. In configuration (E), the strongest upper plate heating exists. Due to

the basic temperature distribution the height of the region of adverse temperature gradient is lower for the case of $\phi_\theta^L = 0.3$ than that for $\phi_\theta^L = 1.0$. Therefore, the critical wave number is higher for $\phi_\theta^L = 0.3$ at $x > 0.025$. When x decreases, the thickness of the thermal boundary layer near the lower plate decreases, and then the critical wave number increases for $\phi_\theta^L = 1.0$. For the thermal boundary condition of $\phi_\theta^L = 0.3$, the upper plate heating is relatively stronger than the lower plate heating. The destabilizing effect of axial convection terms $\phi_u(\partial\theta/\partial x) + u(\partial\phi_\theta/\partial x)$ shown in equation (21) enlarges the unstable region and gives a lower a^* for $\phi_\theta^L = 0.3$ than that for $\phi_\theta^L = 1.0$ near $x = 0.01$. In the region near $x = 0.02$, the destabilizing effect diminishes rapidly, and shows a rapid change of a^*.

6. CONCLUDING REMARKS

(1) In the present study, the lower plate, upper plate and inlet are subjected to three different constant temperatures. The heating of the upper plate causes a thermal stratification, but the heating of the lower plate introduces a thermal destabilization. Three representative unstable heating configurations are selected among the six heating conditions.

(2) The present numerical results utilizing an instability criterion $\partial/\partial t = 0$ with $\partial/\partial x \neq 0$ show good agreement with the existing experimental results. The criterion $\partial/\partial t = 0$ with $\partial/\partial x \neq 0$ determines the neutral stability condition of a growing disturbance in comparison with the criterion $\partial/\partial x = 0$ which determines the critical condition upstream of the growing disturbances. The numerical procedure described here is therefore capable of handling the prediction of the effect of asymmetric heating on thermal instability.

(3) There are different behaviours for the onset of the disturbances for the three representative unstable heating configurations. Variations of the critical Rayleigh number and wave number are summarized in Table 2. The variations of critical wave number for configurations (E) and (F) are complicated. The details are described in Fig. 9(b).

Table 2. Variations of Ra^* and a^* for x, Pr and heating condition

Configuration		x increases	Pr increases	Heating condition†
B	Ra^*	Decreases	Decreases	Increases
	a^*	Decreases	Decreases	Decreases
C (D)	Ra^*	Decreases	Decreases	Increases
	a^*	Decreases	Decreases	Increases
E (F)	Ra^*	Decreases	Decreases	Decreases
	a^*	‡	‡	‡

† B, $\phi_\theta^L = 1.0$, $\phi_\theta^U = 0.0$, $\phi_\theta^I = 0.0$–0.5, 1.0–0.5; C, $\phi_\theta^L = 1.0$, $\phi_\theta^I = 0.0$, $\phi_\theta^U = 0.0$–0.6; D, $\phi_\theta^I = 1.0$, $\phi_\theta^U = 0.0$, $\phi_\theta^L = 1.0$–0.4; E, $\phi_\theta^U = 1.0$, $\phi_\theta^I = 0.0$, $\phi_\theta^L = 0.2$–1.0; F, $\phi_\theta^I = 1.0$, $\phi_\theta^L = 0.0$, $\phi_\theta^U = 0.8$–0.0.

‡ Details are shown in Fig. 9(b).

Acknowledgements—The authors would like to acknowledge the National Science Council, R.O.C., for its support of the present work through project NSC 79-0404-E007-07.

REFERENCES

1. Y. Mori and Y. Uchida, Forced convective heat transfer between horizontal flat plates, *Int. J. Heat Mass Transfer* **9**, 803–817 (1966).
2. W. Nakayama, G. J. Hwang and K. C. Cheng, Thermal instability in plane Poiseuille flow, *J. Heat Transfer* **92**, 61–68 (1970).
3. G. J. Hwang and K. C. Cheng, Convective instability in the thermal entrance region of a horizontal parallel-plate channel heated from below, *J. Heat Transfer* **95**, 72–77 (1973).
4. K. C. Cheng and R. S. Wu, Axial heat conduction effects on thermal instability of horizontal plane Poiseuille flows heated from below, *J. Heat Transfer* **98**, 564–569 (1976).
5. H. V. Mahaney, F. P. Incropera and S. Ramadhyani, Development of laminar mixed convection flow in a horizontal rectangular duct with uniform bottom heating, *Numer. Heat Transfer* **12**, 137–155 (1987).
6. M. Akiyama, G. J. Hwang and K. C. Cheng, Experiments on the onset of longitudinal vortices in laminar forced convection between horizontal plates, *J. Heat Transfer* **93**, 335–341 (1971).
7. S. Ostrach and Y. Kamotani, Heat transfer augmentation in laminar fully developed channel flow by means of heating from below, *J. Heat Transfer* **97**, 220–225 (1975).
8. G. J. Hwang and C. L. Liu, An experimental study of convective instability in the thermal entrance region of a horizontal parallel-plate channel heated from below, *Can. J. Chem. Engng* **54**, 521–525 (1976).
9. Y. Kamotani and S. Ostrach, Effect of thermal instability on thermally developing laminar channel flow, *J. Heat Transfer* **98**, 62–66 (1976).
10. Y. Kamotani, S. Ostrach and H. Miao, Convective heat transfer augmentation in thermal entrance regions by means of thermal instability, *J. Heat Transfer* **101**, 222–226 (1979).
11. F. P. Incropera, A. L. Knox and J. R. Maughan, Mixed-convection flow and heat transfer in the entry region of a horizontal rectangular duct, *J. Heat Transfer* **109**, 434–439 (1987).
12. J. R. Maughan and F. P. Incropera, Experiments on mixed convection heat transfer for airflow in a horizontal and inclined channel, *Int. J. Heat Mass Transfer* **30**, 1307–1318 (1987).
13. K. C. Chiu and F. Rosenberger, Mixed convection between horizontal plates—I. Entrance effects, *Int. J. Heat Mass Transfer* **30**, 1546–1654 (1985).
14. D. G. Osborne and F. P. Incropera, Laminar mixed convection heat transfer for flow between horizontal parallel plates with asymmetric heating, *Int. J. Heat Mass Transfer* **28**, 207–217 (1985).
15. F. P. Incropera and J. A. Schutt, Numerical simulation of laminar mixed convection in the entrance region of horizontal rectangular ducts, *Numer. Heat Transfer* **8**, 707–729 (1985).
16. Y. Kurosaki and I. Satoh, Laminar heat transfer in an asymmetric heated rectangular duct, *Int. J. Heat Mass Transfer* **30**, 1201–1208 (1987).
17. H. V. Mahaney, F. P. Incropera and S. Ramadhyani, Effect of wall heat flux distribution on laminar mixed convection in the entrance region of a horizontal rectangular duct, *Numer. Heat Transfer* **13**, 427–450 (1988).
18. A. Moutsoglou, T. S. Chen and K. C. Cheng, Vortex instability of mixed convection flow over a horizontal flat plate, *J. Heat Transfer* **103**, 257–261 (1981).

19. T. S. Chen, A. Moutsoglou and B. F. Armaly, Thermal instability of mixed convection flow over inclined surfaces, *Numer. Heat Transfer* **5**, 343–352 (1982).
20. J. Y. Yoo, P. Park, K. C. Choi and S. T. Ro, An analysis on the thermal instability of forced convection flow over isothermal horizontal flat plate, *Int. J. Heat Mass Transfer* **30**, 927–935 (1987).
21. F. S. Lee and G. J. Hwang, Transient analysis on the onset of thermal instability in the thermal entrance region of a horizontal parallel plate channel, *J. Heat Transfer* (in press).
22. S. V. Patankar, *Numerical Heat Transfer and Fluid Flow*, Chaps. 5 and 6. Hemisphere, Washington, DC (1980).
23. F. H. Harlow and J. E. Welch, Numerical calculation of time-dependent viscous incompressible flow of fluid with free surface, *Physics Fluids* **8**, 2182–2189 (1965).

EFFET DU CHAUFFAGE ASYMETRIQUE SUR L'APPARITION DE L'INSTABILITE DANS LA REGION D'ENTREE THERMIQUE D'UN CANAL ENTRE PLANS PARALLELES

Résumé—On présente une analyse linéaire dépendante du temps sur l'apparition de l'instabilité d'un écoulement laminaire pleinement établi dans la région d'entrée thermique d'un canal entre plans horizontaux parallèles chauffés asymétriquement, avec le plan inférieur, le plan supérieur et l'entrée à trois températures constantes et différentes. Le chauffage du plan supérieur cause une stratification thermique, mais le chauffage de la plaque inférieure introduit une destabilisation thermique. Avec les trois températures differentes, six configurations de chauffage sont analysées et on montre seulement trois configurations de chauffage instables représentatives. Un critere $\partial/\partial t = 0$ avec $\partial/\partial x \neq 0$, pout la détermination de la condition critique d'apparition des rouleaux de tourbillons longitudinaux, donne des résultats qui s'accordent mieux avec les données expérimentales existantes en comparaison avec le critère $\partial/\partial x = 0$ utilisé précédemment. Les nombres de Rayleigh critiques et les nombres d'onde critiques correspondants pour les trois configurations instables sont présentés avec $Pr = 0{,}7$ et 7,0.

DER EINFLUSS ASYMMETRISCHER BEHEIZUNG AUF DAS EINSETZEN DER THERMISCHEN INSTABILITÄT IM EINTRITTSBEREICH EINES KANALS AUS PARALLELEN PLATTEN

Zusammenfassung—Es wird eine zeitabhängige lineare Analyse über das Einsetzen der thermischen Instabilität in einer voll ausgebildeten laminaren Strömung im Eintrittsbereich eines asymmetrisch beheizten Kanals aus waagerechten parallelen Platten vorgestellt. Die untere Platte, die obere Platte und das Eintrittsgebiet befinden sich auf einer jeweils unterschiedlichen konstanten Temperatur. Die Beheizung der oberen Platte bewirkt eine thermische Schichtung, wogegen die Beheizung der unteren Platte eine thermische Destabilisierung hervorruft. Mit den drei unterschiedlichen Platten- und Einlaßtemperaturen werden sechs Heizungsanordnungen für den waagerechten Kanal untersucht, wobei sich nur drei der Anordnungen als instabil erweisen. Es wird ein Kriterium für das Einsetzen von Längswirbeln angegeben ($\partial/\partial t = 0$ bei $\partial/\partial x \neq 0$). Die damit gefundenen Ergebnisse stimmen gut mit vorhandenen Versuchsdaten überein. Abschließend wird die kritische Rayleigh-Zahl und die entsprechende kritische Wellenzahl für die drei instabilen Heizungsanordnungen für $Pr = 0{,}7$ und 7,0 vorgestellt.

ВЛИЯНИЕ АСИММЕТРИЧНОГО НАГРЕВА НА ВОЗНИКНОВЕНИЕ ТЕПЛОВОЙ НЕУСТОЙЧИВОСТИ НА НАЧАЛЬНОМ ТЕПЛОВОМ УЧАСТКЕ ПЛОСКОПАРАЛЛЕЛЬНОГО КАНАЛА

Аннотация—Дан нестационарный линейный анализ возникновения тепловой неустойчивости полностью развитого ламинарного течения во входной области асимметрично нагреваемого горизонтального плоскопараллельного канала, в котором входной участок, верхняя и нижняя стенки поддерживаются при трех различных постоянных температурах. Нагрев верхней стенки вызывает тепловую стратификацию, в то время как нагрев нижней приводит к тепловой неустойчивости. При трех различных температурах входного участка, а также верхней и нижней стенок анализируются шесть конфигураций нагрева канала и показано, что только три из них характеризуются неустойчивым режимом. При критических условиях возникновения продольных вихревых валов в виде $\partial/\partial t = 0$ и $\partial/\partial x \neq 0$ получены результаты, которые лучше согласуются с имеющимися экспериментальными данными по сравнению с используемым ранее приближением $\partial/\partial x = 0$. Приводятся критические числа Рэлея и соответствующие волновые числа для трех конфигураций неустойчивого режима при $Pr = 0{,}7$ и 7,0.